



X International Conference on Structural Dynamics, EURODDYN 2017

## Performance of a dual-stage inerter-based vibration isolator

Jian Yang<sup>a,\*</sup>, Jason Z. Jiang<sup>b</sup>, Xiang Zhu<sup>c</sup>, Hao Chen<sup>a</sup>

<sup>a</sup>Department of Mechanical, Materials and Manufacturing Engineering, University of Nottingham Ningbo China, Ningbo 315100, China

<sup>b</sup>Department of Mechanical Engineering, University of Bristol, Queen's Building, University Walk, Bristol, BS8 1TR, UK

<sup>c</sup>School of Naval Architecture and Ocean Engineering, Huazhong University of Science and Technology, Wuhan 430074, China

### Abstract

This paper investigates the dynamic behaviour and performance of a dual-stage inerter-based vibration isolator. Force transmissibility and vibration power flow variables are used as performance indices to evaluate the effectiveness of the inerter-based vibration isolator. Vibration power input, transmission and dissipation characteristics of the system are examined. It is found that the inclusion of inerters in dual-stage vibration isolator can reduce force and vibration power flow transmission over a larger band of excitation frequencies. The addition of inerters can also introduce notches in the curves of force transmissibility and time-averaged transmitted power such that the vibration transmission may be greatly suppressed at pre-determined excitation frequencies. These findings demonstrate the potential benefits of employing inerters in vibration isolation and facilitate better understanding of vibration mitigation systems with such element.

© 2017 The Authors. Published by Elsevier Ltd.

Peer-review under responsibility of the organizing committee of EURODDYN 2017.

**Keywords:** inerter; vibration isolator; force transmissibility; vibration power flow; dual-stage vibration isolator

### 1. Introduction

Vibration isolators have been widely used to reduce the transmission of excessive vibrations from a vibrating source to a receiving structure. The design methodology of conventional spring-damper isolators has been well-documented. To achieve better vibration mitigation performance, new designs of vibration isolators with inclusion of nonlinear or novel linear elements have received growing attention [1,2].

Recently, a passive mechanical element - the inerter, was proposed which has the property that the forces applied are proportional to the relative acceleration across its terminals, i.e.,  $F_b = b(\dot{V}_1 - \dot{V}_2)$ , where  $F_b$  is the coupling inertial force,  $b$  is a intrinsic parameter of the inerter named inertance,  $V_1$  and  $V_2$  are the accelerations of the two ends [3]. Thus this device can be used to change to dynamic property of a dynamical system such that the vibration transmission characteristics can be modified. The device has been used in the design of railway vehicle suspension systems [4,5], aircraft landing gear shimmy suppression [6,7] and building vibration control systems [8]. Some studies have also been reported on the performance of single degree-of-freedom (DOF) vibration isolators with inerters [9,10].

\* Corresponding author. Tel.: +86-574-88180000-3141 ; fax: +86-574-88180175.

E-mail address: [jian.yang@nottingham.edu.cn](mailto:jian.yang@nottingham.edu.cn)

Vibration power flow analysis (PFA) method is a widely-accepted tool to characterise the dynamic behaviour of coupled systems and complex structures [11]. Various PFA approaches has been developed to investigate linear vibration control systems. The power flow characteristics of single DOF inerter-based isolators were also investigated [10]. In recent years, PFA methods have been developed to examine the power flow behaviour of nonlinear dynamical systems [12–14].

In this paper, the performance of a dual-stage inerter-based vibration isolator is investigated via examination of its force transmissibility and vibration power flow behaviour. The paper is organised as follows. The dual-stage vibration isolator will be briefly introduced and modelled in the next section. Then the force transmissibilities of the system will be derived analytically in Section 3. The vibration power flow variables and kinetic energies of the system will be formulated in Section 4. Case studies on force transmissibility and power flow behaviour of the system are performed with results presented in Sections 3 and 4, respectively. Conclusions are provided at the end of the paper.

### 2. The dual-stage vibration isolator model

Fig. 1 shows a schematic representation of the model, which includes a lower stage with a mass  $m_1$  and a lower spring-damper-inerter (SDI) unit, on which an upper stage with a mass  $m_2$  is mounted via an upper SDI unit. The lower SDI consists of a spring of stiffness coefficient  $k_1$ , a damper of damping coefficient  $c_1$  and an inerter of inertance  $b_1$  connected in parallel, while the upper SDI comprises a spring of stiffness  $k_2$ , a damper of damping coefficient  $c_2$  and an inerter of inertance  $b_2$ . Mass  $m_2$  is subject to a harmonic force excitation with amplitude  $f_0$  and frequency  $\omega$ . The static equilibrium state of the system is used as a reference such that the corresponding displacements of the masses  $x_1 = x_2 = 0$ .

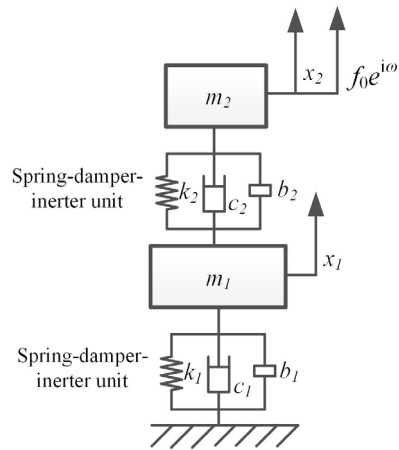


Fig. 1. A schematic representation of a dual-stage inerter-based vibration isolator.

The dynamic governing equation of the system is

$$\begin{pmatrix} m_1 + b_1 + b_2 & -b_2 \\ -b_2 & m_2 + b_2 \end{pmatrix} \begin{pmatrix} \ddot{x}_1 \\ \ddot{x}_2 \end{pmatrix} + \begin{pmatrix} c_1 + c_2 & -c_2 \\ -c_2 & c_2 \end{pmatrix} \begin{pmatrix} \dot{x}_1 \\ \dot{x}_2 \end{pmatrix} + \begin{pmatrix} k_1 + k_2 & -k_2 \\ -k_2 & k_2 \end{pmatrix} \begin{pmatrix} x_1 \\ x_2 \end{pmatrix} = \begin{pmatrix} 0 \\ f_0 e^{i\omega t} \end{pmatrix} \tag{1}$$

It shows that the addition of inerters changes the mass matrix, i.e., it modifies the inertia properties of the system. Assuming that the steady-state displacements of masses  $m_1$  and  $m_2$  are  $x_1 = x_{10}e^{i\omega t}$ ,  $x_2 = x_{20}e^{i\omega t}$ , respectively, where  $x_{10}$  and  $x_{20}$  are complex amplitudes of the displacements. The solution to Eq. (1) can be found to be

$$x_{10} = \frac{-d_{12}f_0}{\det(D)}, x_{20} = \frac{d_{11}f_0}{\det(D)}$$

where  $\det(D) = d_{11}d_{22} - d_{12}d_{21}$  is the determinant of the dynamic stiffness matrix  $D$ :

$$D = \begin{pmatrix} d_{11} & d_{12} \\ d_{21} & d_{22} \end{pmatrix} = D = \begin{pmatrix} (k_1 + k_2) - \omega^2(m_1 + b_1 + b_2) + i\omega(c_1 + c_2) & \omega^2 b_2 - i\omega c_2 - k_2 \\ \omega^2 b_2 - i\omega c_2 - k_2 & k_2 - \omega^2(m_2 + b_2) + i\omega c_2 \end{pmatrix}$$

### 3. Force transmissibility

As the force transmissibility is defined as the ratio between the amplitude of the transmitted force and that of the external force, we have

$$TR_1 = \left| \frac{f_{i1}}{f_0} \right| = \frac{\sqrt{(k_2 - \omega^2 b_2)^2 + (\omega c_2)^2} \sqrt{(k_1 - \omega^2(m_1 + b_1))^2 + (\omega c_1)^2}}{|\det(D)|}, \quad (2)$$

$$TR_2 = \left| \frac{f_{i2}}{f_0} \right| = \frac{\sqrt{(k_2 - \omega^2 b_2)^2 + (\omega c_2)^2} \sqrt{(k_1 - \omega^2 b_1)^2 + (\omega c_1)^2}}{|\det(D)|}, \quad (3)$$

for the force transmissibility to mass  $m_1$  and that to the ground, respectively. Eqs. (2) and (3) show that for the undamped system (i.e.,  $c_1 = c_2 = 0$ ) with inerters, there will be no force transmission from the upper stage to mass  $m_1$  at two excitation frequencies, one locating at  $\omega = \sqrt{k_2/b_2}$  and another at  $\omega = \sqrt{k_1/(b_1 + m_1)}$ . Thus anti-resonances may be identified in the force transmissibility curve of  $TR_1$ . In contrast, for the undamped system with only springs and dampers, the force transmissibility  $TR_1$  will be zero only at a single frequency of  $\omega = \sqrt{k_1/m_1}$ . There are also anti-resonances locating at  $\omega = \sqrt{k_1/b_1}$  and  $\omega = \sqrt{k_2/b_2}$  in the force transmissibility  $TR_2$ . At these two excitation frequencies, the force transmission to the fixed ground is zero. This behaviour demonstrates that inerters can be introduced to vibration isolators so as to place notches in force transmissibility curves at pre-determined excitation frequencies such that the corresponding level of force transmission can be significantly reduced. It should also be noted that on the left-hand side of Eqs. (2) and (3), the highest order of the non-dimensional excitation frequency  $\omega$  of the denominator and numerator are the same. Therefore, as the excitation frequency tends to infinity, the force transmissibility  $TR_1$  and  $TR_2$  will tend to

$$\lim_{\omega \rightarrow \infty} TR_1 = \frac{b_2(m_1 + b_1)}{(m_1 + b_1)(m_2 + b_2) + b_2 m_2} < 1, \quad \lim_{\omega \rightarrow \infty} TR_2 = \frac{b_1 b_2}{(m_1 + b_1)(m_2 + b_2) + b_2 m_2} < 1.$$

These expressions show that there are asymptotic values of the force transmissibilities when the non-dimensional excitation frequency  $\omega$  increases to high frequencies. The limit value of  $TR_1$  will not be zero when  $b_2 \neq 0$ . Similarly,  $TR_2$  will tend to a finite value when  $b_1 \neq 0$  and  $b_2 \neq 0$ . Moreover, a mathematical examination shows that these limit values will remain smaller than one, suggesting that at high frequencies the transmitted force amplitudes are smaller than that of the original excitation force. Therefore, the inerter-based vibration isolator can still reduce force transmission at high excitation frequencies.

Fig. 2 illustrates the effects of inerters on vibration isolation performance in terms of force transmissibility. The system parameter values are set to be  $m_1 = 20$  kg,  $m_2 = 10$  kg,  $c_1 = 0.4$  Ns/m,  $c_2 = 0.1$  Ns/m,  $k_1 = 20$  N/m,  $k_2 = 2.5$  N/m and  $f_0 = 10$  N. The force transmission characteristics of the system with conventional dual-stage isolator without inerters (i.e.,  $b_1 = b_2 = 0$ , Case one) are firstly obtained. Two undamped natural frequencies of this system are found to be  $\omega = \omega_1 = 0.464$  Hz and  $\omega = \omega_2 = 1.077$  Hz. Correspondingly, two peaks can be identified on the corresponding curves of force transmissibility  $TR_1$  and  $TR_2$ . To reduce these peak values, one possible approach is to introduce notches by introducing inerters to the dual-stage isolator. The values of  $b_1$  and  $b_2$  can be chosen such that the anti-resonance frequencies locate approximately at the original natural frequencies of the system without inerters. As weakly damped systems are considered here, the anti-resonance frequencies may be approximated by those of the corresponding undamped system. Thus the values of  $b_1$  and  $b_2$  are set such that  $\sqrt{k_1/(b_1 + m_1)} = \omega_1$  and  $\sqrt{k_2/b_2} = \omega_2$ . Correspondingly  $b_1 = 3.645m_1$  and  $b_2 = 0.216m_2$  (i.e., Case two). The force transmissibility characteristics of two other cases with  $b_1 = 3.645m_1$ ,  $b_2 = 0$  (i.e., Case three) and  $b_1 = 0$ ,  $b_2 = 0.216m_2$  (i.e., Case four) are also included in Fig. 2 for comparison. It shows that with use of the dual-stage inerter-based vibration isolator in Case two, the force transmissibilities  $TR_1$  and  $TR_2$  are significantly reduced from the original values of the system with a conventional dual-stage isolator in Case one. The addition of inerters in vibration isolator also shifts the peaks to the low-frequency range. This is beneficial as the frequency range of effective isolation is enlarged. It is seen that in the low-frequency range with  $\omega < 0.3$ , the force transmissibility curves of the four cases considered merge, indicating that the corresponding effects of inerters on force transmission are relatively small. The figure also shows that at high excitation frequencies, the inerter-based vibration isolators are not as effective in the isolation of force transmission, compared with the Case one with a conventional vibration isolator. It is also seen that towards higher

excitation frequency, both  $TR_1$  and  $TR_2$  tend to an asymptotic values. It is worth noticing that the force transmissibility will still be smaller than 1 at high frequencies, indicating that the force transmission is still attenuated.

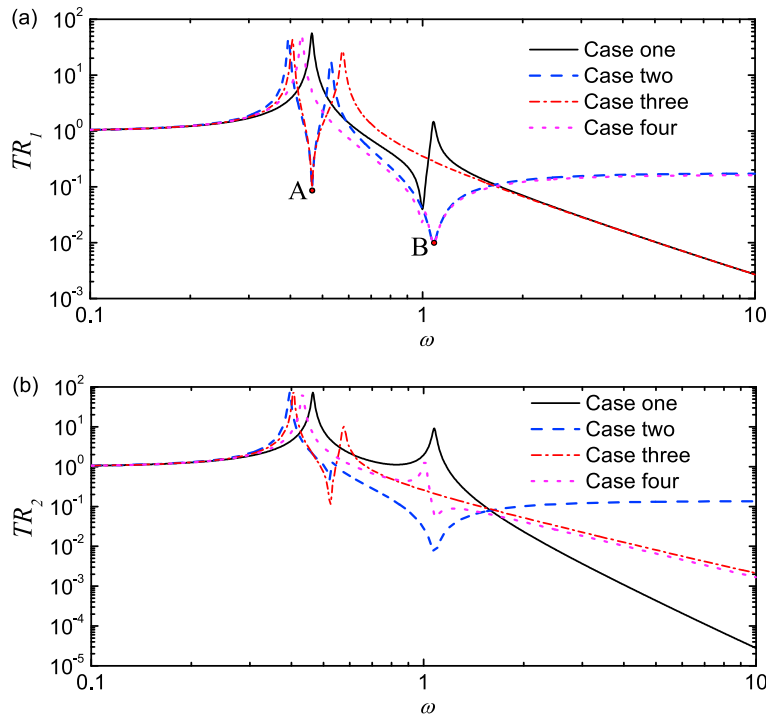


Fig. 2. The force transmissibility behaviour of a dual-stage inerter-based vibration isolator.

#### 4. Vibration power flow analysis

In this section, the vibration transmission behaviour of the 2DOF system with inerter-based linear isolators is examined from the viewpoint of vibration power and energy. The equation of power balance is obtained by pre-multiplying both sides of Eq. (1) by the velocity vector:

$$\dot{K} + \dot{U} + p_d = p_{in} \tag{4}$$

where

$$\dot{K} = \begin{pmatrix} \dot{x}_1 \\ \dot{x}_2 \end{pmatrix}^T \begin{pmatrix} m_1 + b_1 + b_2 & -b_2 \\ -b_2 & m_2 + b_2 \end{pmatrix} \begin{pmatrix} \dot{x}_1 \\ \dot{x}_2 \end{pmatrix}, \dot{U} = \begin{pmatrix} \dot{x}_1 \\ \dot{x}_2 \end{pmatrix}^T \begin{pmatrix} k_1 + k_2 & -k_2 \\ -k_2 & k_2 \end{pmatrix} \begin{pmatrix} x_1 \\ x_2 \end{pmatrix}, p_d = \begin{pmatrix} \dot{x}_1 \\ \dot{x}_2 \end{pmatrix}^T \begin{pmatrix} c_1 + c_2 & -c_2 \\ -c_2 & c_2 \end{pmatrix} \begin{pmatrix} \dot{x}_1 \\ \dot{x}_2 \end{pmatrix}, p_{in} = \begin{pmatrix} \dot{x}_1 \\ \dot{x}_2 \end{pmatrix}^T \begin{pmatrix} 0 \\ f_0 e^{i\omega t} \end{pmatrix}$$

are the rates of change of kinetic and potential energies, and the instantaneous dissipated and input powers, respectively. The superscript 'T' denotes transpose matrix. As the introduction of inerter changes the mass matrix, it directly varies the characteristics of the kinetic energy of the system. Note that over a cycle of steady-state oscillation, there will be no net change in the mechanical energy of the system. The corresponding time-averaged input power  $p_{in}$  into the system and time-averaged transmitted power  $\bar{p}_t$  to mass  $m_1$  are

$$\bar{p}_{in} = \bar{p}_d = \frac{1}{2} \{f_{d1} v_{10}^*\} + \frac{1}{2} \{f_{d2} (v_{20} - v_{10})^*\} = \frac{\omega^2 |f|^2 (c_1((k_2 - \omega^2 b_2)^2 + (\omega c_2)^2) + c_2((k_1 - \omega^2(m_1 + b_1))^2 + (\omega c_1)^2))}{2|\det(D)|^2}, \tag{5}$$

$$\bar{p}_t = \bar{p}_{d1} = \frac{1}{2} \{f_{d1} v_{10}^*\} = \frac{c_1 \omega^2 |f|^2 ((k_2 - \omega^2 b_2)^2 + (\omega c_2)^2)}{2|\det(D)|^2}, \tag{6}$$

respectively, where  $f_{d1} = i\omega c_1 x_{10}$  and  $f_{d2} = i\omega c_2(x_{20} - x_{10})$  are the complex amplitudes of the damping force of the damper  $c_1$  and that of the damper  $c_2$ , respectively;  $v_{10} = i\omega x_{10}$  and  $v_{20} = i\omega x_{20}$  are the complex amplitudes of the velocities of mass  $m_1$  and  $m_2$ , respectively. Eq. (6) suggests that for weakly damped system, the amount of time-averaged transmitted power  $p_t$  to mass  $m_1$  may be expected to be small at  $\omega = \sqrt{k_2/b_2}$ . The time-averaged transmitted power to the fixed ground is zero.

The power transmission ratio  $R_t$  to mass  $m_1$  may be defined as the ratio between the time-averaged transmitted power  $\bar{p}_t$  and the time-averaged input power  $\bar{p}_{in}$ :

$$R_t = \frac{\bar{p}_t}{\bar{p}_{in}} = \frac{c_1((k_2 - \omega^2 b_2)^2 + (\omega c_2)^2)}{c_1((k_2 - \omega^2 b_2)^2 + (\omega c_2)^2) + c_2((k_1 - \omega^2(m_1 + b_1))^2 + (\omega c_1)^2)} \tag{7}$$

Note that both the numerator and denominator are of the same order of excitation frequency  $\omega$ . When moving towards high frequencies,  $R_t$  takes the limit of

$$\lim_{\Omega \rightarrow \infty} R_t = \frac{c_1 b_2^2}{c_1 b_2^2 + c_2(m_1 + b_1)^2} \tag{8}$$

Clearly when  $\lambda_2 \neq 0$ , the limit of power transmission ratio is a finite value. It suggests that at high frequencies, a fixed relative portion of the input power is transmitted to the lower stage of the isolator. Based on these formulations, Fig. 3 investigates the effects of introducing a dual-stage inerter-based vibration isolator on the power flow behaviour.

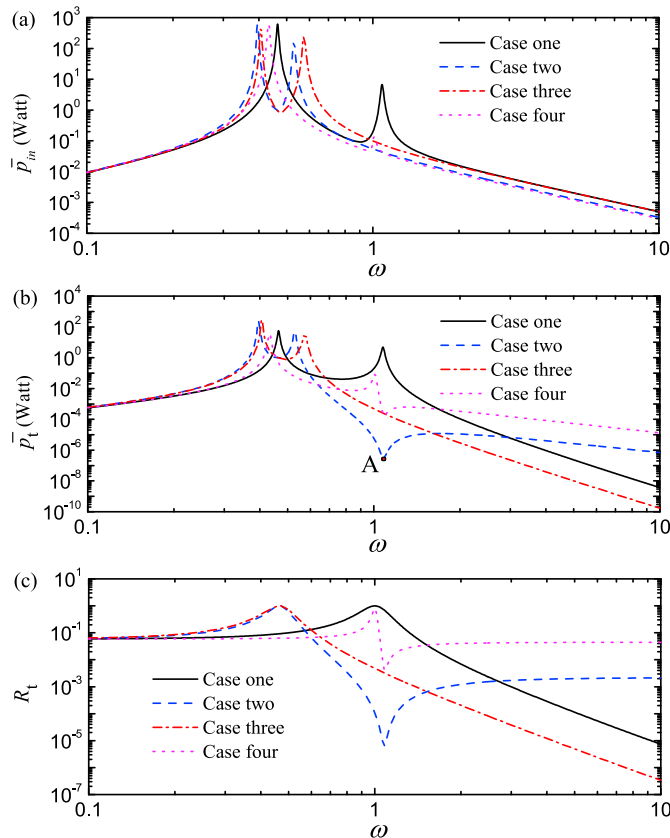


Fig. 3. The time-averaged power flow behaviour of a dual-stage inerter-based vibration isolator.

The system parameter values are set to be the same as those used in Fig. 2. In Case one,  $b_1 = b_2 = 0$ , i.e., two conventional vibration isolators are used. In Case two, the inertance ratios  $b_1 = 3.645m_1, b_2 = 0.216m_2$  two inerter-based vibration isolators are employed. Cases three and four are with  $b_1 = 3.645m_1, b_2 = 0$  and  $b_1 = 0, b_2 = 0.216m_2$ ,

respectively. The former and the latter consider the use inerter in the lower stage and the upper, respectively. Figs. 3(a) and (b) show that comparing with Case one, the inclusions of inerter-based vibration isolator in Case two result in the shift of the peaks in time-averaged input and transmitted powers to the low-frequency range. This is beneficial for vibration isolation. Fig. 3(a) shows that the original peak values the time-averaged transmitted power  $\bar{p}_t$  in Case one are also significantly reduced by the addition of inerters to the upper and lower stages. The anti-peak point A in Fig. 3(b) shows that the power transmission to the lower stage can be greatly attenuated by employing inerter-based isolator. In the low-frequency range, the influence of inerters on time-averaged power flows is observed to be small. In the high-frequency range, it is seen that adding inerters reduces time-averaged input power but increases the time-averaged transmitted power. Fig. 3(c) plots the power transmission ratio, which represents the relative portion of vibration power transmitted to the lower stage in the total input power. It shows that the use of inerter-based vibration isolators brings about a larger  $R_a$  at low excitation frequencies. However at a higher frequency, an anti-peak notch in  $R_a$  is observed and introduction of inerters assists in reduction of power transmission ratio. In the high-frequency range,  $R_a$  becomes larger after adding inerters. With further increases in the excitation frequency  $\omega$ , the power transmission ratio tends to an asymptotic value, which has been formulated analytically in Eq. (8).

## 5. Conclusions

The dynamics and performance of a dual-stage inerter-based vibration isolator were investigated in this paper. The force transmissibility and vibration power flow characteristics of the system were examined to evaluate the effects of the inclusion of inerter on the suppression of vibration transmission. It was found that the inclusion of inerters can provide benefits to vibration mitigation by creating a large frequency band where the force transmissibility is relatively low. The addition of inerters in the isolator also introduced anti-resonances. Based on this property, force transmissibility and time-averaged power flow transmission can be greatly suppressed at pre-determined excitation frequencies. It was also found that there exists asymptotic behaviour of force transmission and power transmission ratio when the excitation frequency extends to high frequencies.

## Acknowledgements

This work was supported by National Natural Science Foundation of China [Grant Number 51605233] and the Science and Technology Bureau of Ningbo, China [Grant number 2015A610094].

## References

- [1] R. A. Ibrahim, Recent advances in nonlinear passive vibration isolators, *J. Sound Vib.* 314 (2008) 371–452.
- [2] J. Yang, Y. P. Xiong, J. T. Xing, Dynamics and power flow behaviour of a nonlinear vibration isolation system with a negative stiffness mechanism, *J. Sound Vib.* 332(1) (2013) 167–183.
- [3] M. C. Smith, Synthesis of mechanical networks: The inerter, *IEEE T. Automat. Contr.* 47(10) (2002) 1648–1662.
- [4] F.C. Wang, M.K. Liao, B.H. Liao, W.J. Sue, H.A. Chan, The performance improvements of train suspension systems with mechanical networks employing inerters, *Vehicle Syst. Dyn.* 47 (7) (2009) 805–830.
- [5] J. Z. Jiang, A. Z. Matamoros-Sanchez, R. M. Goodall, M. C. Smith, Passive suspensions incorporating inerters for railway vehicles, *Vehicle Syst. Dyn.* 50 (Suppl. 1) (2012) 263–276.
- [6] X. Dong, Y. Liu, M.Z.Q. Chen, Application of inerter to aircraft landing gear suspension, *Proceedings of the 34th Chinese Control Conference (CCC 2015)*, Hangzhou, China, July 2015, pp.2066–2071.
- [7] Y. Li, J. Z. Jiang, S. Neild, Inerter-based configurations for main landing gear shimmy suppression, *J. Aircraft* 54(2)(2017) 684–693.
- [8] S. Y. Zhang, J. Z. Jiang, N. Simon, Optimal configurations for a linear vibration suppression device in a multi-storey building, *Struct. Control Hlth.* 24 (2017) DOI: 10.1002/stc.1887.
- [9] Y. Hu, M. Z. Q. Chen, Z. Shu, L. Huang, Analysis and optimisation for inerter-based isolators via fixed-point theory and algebraic solution, *J. Sound Vib.* 346 (2015)17-36
- [10] J. Yang, Force transmissibility and vibration power flow behaviour of inerter-based vibration isolators, *J. Phys. Conf. Ser.* 744 (2016) 012234.
- [11] H. G. D. Goyder, R. G. White, Vibration power flow from machines into built-up structures, *J. Sound Vib.* 68 (1980) 59–117.
- [12] J. Yang, Y. P. Xiong, J. T. Xing, Nonlinear power flow analysis of the Duffing oscillator, *Mech. Syst. Signal Pr.* 45(2) (2014) 563–578.
- [13] J. Yang, Y. P. Xiong, J. T. Xing, Power flow behaviour and dynamic performance of a nonlinear vibration absorber coupled to a nonlinear oscillator, *Nonlinear Dyn.* 80 (3) (2015) 1063–1079.
- [14] J. Yang, Y. P. Xiong, J. T. Xing, Vibration power flow and force transmission behaviour of a nonlinear isolator mounted on a nonlinear base, *Int. J. Mech. Sci.* 115–116 (2016) 238-252.